

## The Pacific–Antarctic Ridge–Foundation hotspot interaction: a case study of a ridge approaching a hotspot

M. Maia<sup>a,\*</sup>, D. Ackermann<sup>b,1</sup>, G.A. Dehghani<sup>c,1</sup>, P. Gente<sup>a,1</sup>, R. Hékinian<sup>d,1</sup>, D. Naar<sup>e,1</sup>,  
J. O'Connor<sup>f,1</sup>, K. Perrot<sup>a,1</sup>, J. Phipps Morgan<sup>g,1</sup>, G. Ramillien<sup>h,1</sup>, S. Révillon<sup>i,1</sup>,  
A. Sabetian<sup>d,1</sup>, D. Sandwell<sup>g,1</sup>, P. Stoffers<sup>b,1</sup>

<sup>a</sup>UMR 6538 CNRS, IUEM, Université de Bretagne Occidentale, Plouzané, France

<sup>b</sup>GPI, Universität Kiel, Kiel, Germany

<sup>c</sup>Institut für Geophysik, Universität Hamburg, Hamburg, Germany

<sup>d</sup>IFREMER, DRO-GM, Plouzané, France

<sup>e</sup>University of South Florida, St. Petersburg, USA

<sup>f</sup>GEOMAR, Kiel, Germany

<sup>g</sup>SCRIPPS Institution of Oceanography, La Jolla, USA

<sup>h</sup>GRGS-CNRS, Toulouse, France

<sup>i</sup>UPR 4661 CNRS, Université de Rennes, Rennes, France

Received 19 October 1999; accepted 6 March 2000

### Abstract

The Foundation hotspot–Pacific–Antarctic Ridge (PAR) system is the best documented case of a fast spreading ridge approaching a hotspot and interacting with it. The morphology, crustal structure inferred from gravity anomalies and the chemical composition of the lavas of the axial area of the PAR show evidence of the influence of the hotspot, that is presently located roughly 35 km west of the spreading ridge axis. Along-axis variation in the Mantle Bouguer anomaly is about 28 mGal, corresponding to a crustal thickening of 1.5 km where the hotspot is nearer to the PAR. Anomalous ridge elevation is 650 m and the along-axis width of the chemical anomaly is 200 km. A comparison of these axial parameters with those derived for other ridge–hotspot systems, suggests that the amount of plume material reaching the ridge axis is smaller for the Foundation–PAR system. This implies a weaker connection between the plume and the ridge. Cumulative effects of a fast spreading rate and of a fast ridge–hotspot relative motion can be responsible for this weak plume–ridge flow. The flow from the hotspot may be less efficiently channelled towards the ridge axis when a fast ridge is rapidly moving towards a hotspot. © 2000 Elsevier Science B.V. All rights reserved.

**Keywords:** Mid-oceanic ridge; Hotspot; Gravity; Bathymetry

### 1. Introduction

Mid-oceanic ridges and hotspots being ubiquitous features, are likely to strongly condition upper mantle thermal structure and dynamics. The interaction processes between mid-oceanic ridges and hotspots have been studied in different geodynamic contexts

\* Corresponding author. Tel.: + 33-2-98-49-8719; fax: + 33-2-98-49-8760.

E-mail address: marcia@univ-brest.fr (M. Maia).

<sup>1</sup> Member of the “Foundation Hotline” Cruise Party.

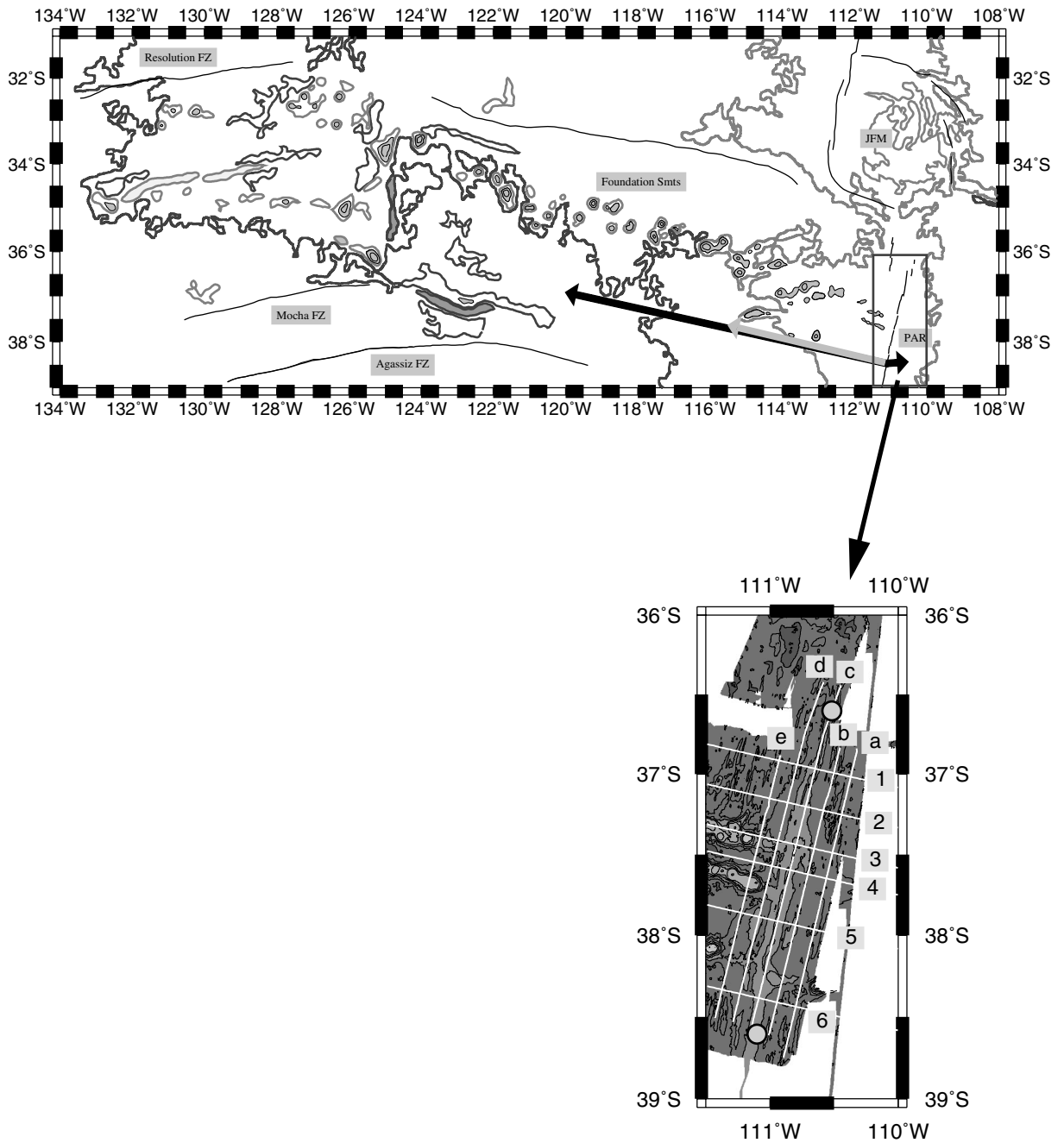


Fig. 1. Simplified predicted bathymetry (Sandwell and Smith, 1997) showing the location and setting of the Foundation seamounts. Light grey isobath is the 3000 m contour and dark grey isobath is the 4000 m contour. Thin black lines with light grey shading show depths below 1000 m. The thick black arrows depict the absolute motion of the Pacific and Antarctic plates and the light grey arrow the absolute motion of the Pacific–Antarctic Ridge. The inset shows the multibeam bathymetry of the axial area with the location of the profiles (letters and numbers) and the dredges (grey circles) discussed in the paper.

(e.g. Morgan, 1978; Schilling, 1985, 1991; Small, 1995) in order to obtain information on the thermal parameters of mantle plumes and mid-oceanic ridges, and on styles of mantle convection. Ridge–hotspot interactions can occur in three different settings: a ridge approaching a hotspot, a ridge centred above a hotspot and a ridge moving away from a hotspot. Nearly all the previous studies have dealt with the ridge-centred case or the case of a ridge moving away from a hotspot. Classical examples of ridge-centred hotspot interactions are the couples Iceland/Mid-Atlantic Ridge (Schilling, 1973; Vogt, 1971) and Azores/Mid-Atlantic Ridge (Vogt, 1976). Numerous examples of ridges moving away from a hotspot, but still maintaining a connecting flow have also been studied. Among them are the Galapagos/Cocos Ridge (Morgan, 1978; Schilling et al., 1982), the Reunion/Central Indian Ridge (Morgan, 1978) and the Ascension/South Atlantic Ridge (Hanan et al., 1985; Schilling et al., 1985) and Easter (Kingsley and Schilling, 1998; Pan and Batiza, 1998). Geochemical and geophysical studies yielded the so-called MRS–MPS model (Migrating Ridge Sink–Mantle Plume Source) (Schilling, 1985) where the ridge acts as a sink draining the plume material along a narrow sub-lithospheric channel. The surface expression of such a flow is a series of topographic highs, linking the present location of the hotspot and the ridge, and made up either of long, linear volcanic ridges or of lined up volcanic edifices (Morgan, 1978; Small, 1995). The chemical composition of rocks sampled along these volcanic features shows a mixing between the two source materials, plume and accreting ridge, following a roughly linear trend between the hotspot and the ridge axis (Haase et al., 1996; Kingsley and Schilling, 1998). As volcanism can occur all along the channel, the ages of the various edifices show no regular progression towards the ridge (Kingsley and Schilling, 1998). The ridge axis also reflects the influence of the neighbouring hotspot. The chemical composition of the lavas shows signs of plume enrichment. Anomalous topography and thick crust have also been reported (Schilling, 1985; Ito and Lin, 1995a,b). Along-axis gradients in these parameters were used to estimate hotspot temperatures and fluxes (Schilling, 1991; Ito et al., 1997; Ribe and Delattre, 1998) as well as the evolution of the ridge–hotspot interaction through time (Ito and Lin, 1995a,b).

The case of a ridge approaching a hotspot has been comparatively less studied due to lack of data for such a system. Two potential candidates are the Louisville/Pacific–Antarctic Ridge (PAR) and the Foundation/Pacific–Antarctic Ridge (Small, 1995; Devey et al., 1997). Recently, the Hollister ridge, believed to be the surface expression of the channel flow between Louisville and the Pacific–Antarctic Ridge (Small, 1995) was found to be of a more complex origin (Géli et al., 1998). Although the chemical and thermal influence of the Louisville hotspot at the PAR axis is undeniable (Castillo et al., 1998), this system clearly deserves further attention. This makes the Foundation/Pacific–Antarctic Ridge system the most favourable location to conduct a comprehensive study of the interactions between a hotspot and an approaching ridge (Devey et al., 1997). In this paper we will present the first interpretation of morphological and geophysical data for the PAR–Foundation system, where the spreading ridge approaches the hotspot at a rate of 43 mm/yr (Maia et al., 1999). These data were obtained in January/February 1997, during a cruise on board the *NO L'Atalante*, led by CNRS–University of Western Brittany. The main objective of this cruise was the complete mapping of the zone of interaction between the Foundation hotspot and the Pacific–Antarctic Ridge. This paper will be focused on the study of the near-axis crustal structure and on discussing the implications of this structure on ridge–hotspot interactions. The petrology and geochemistry as well as the study of the off-axis volcanoes will be reported in other papers by the members of the scientific party. We will show that the influence of the Foundation hotspot in the PAR axial area is specific to the case of a fast spreading ridge approaching a hotspot.

## 2. Geodynamical setting

The Foundation Seamounts (Fig. 1) are located in the South Pacific between 33°S, 131°W and 38°S, 111°W, roughly following a N110° trend (Mammerickx, 1992). At its south eastern end, it intersects the axis of the Pacific–Antarctic Ridge. Volcano ages decrease progressively eastward, from 21 m.y. to very recent ages (O'Connor et al., 1998). This, together with the evolution of basalt compositions (Hémond and Devey, 1996; Devey et al., 1997;

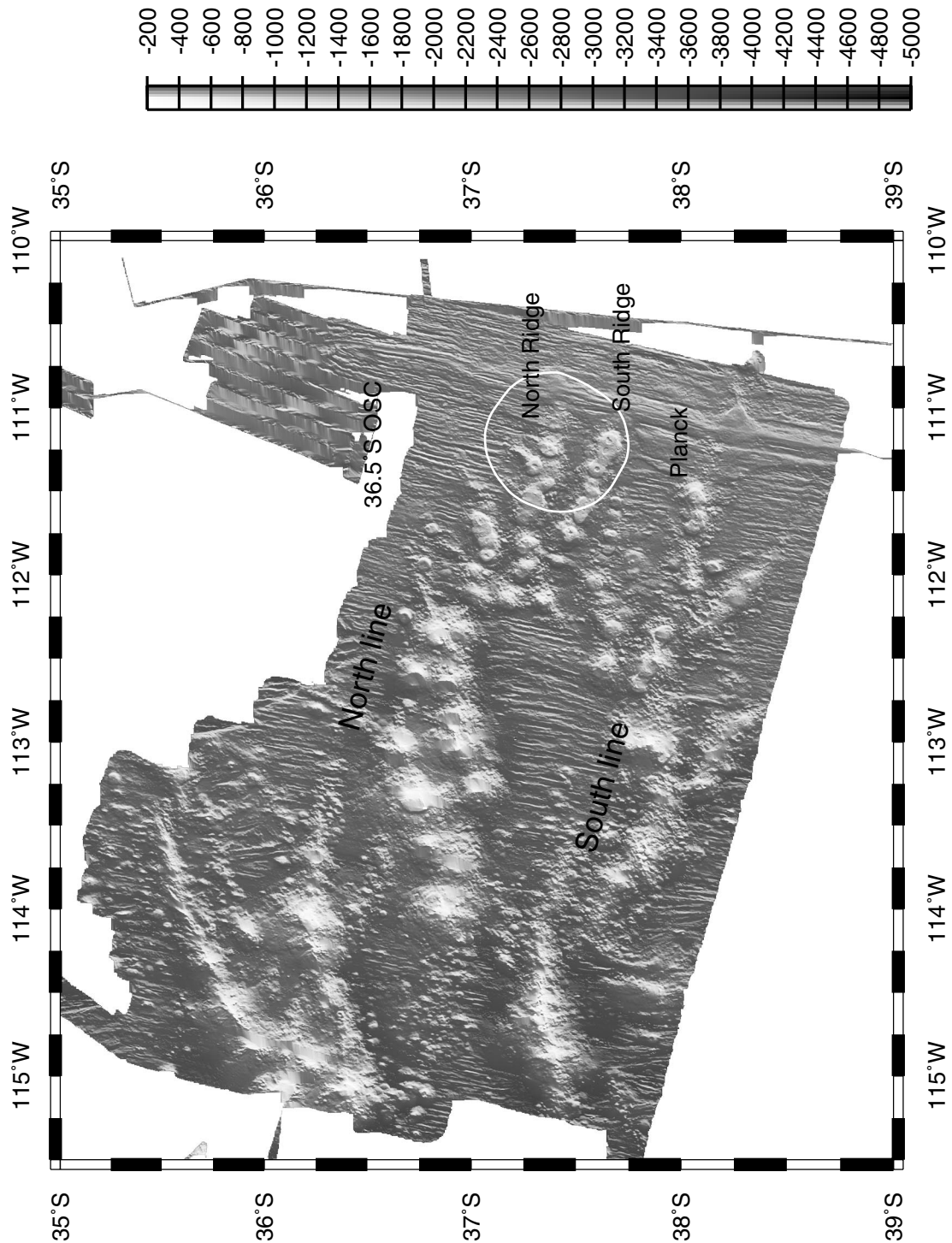


Fig. 2. Shaded multibeam bathymetry of the Foundation seamounts at the ridge-hotspot interaction zone. Depths are shown in a grey shaded scale. The white circle represents the 10 cm contour of the geoid anomaly, taken from Maia et al. (1999). Note the change in the morphology towards the axis of the ridge.

Hékinian et al., 1997) strongly suggests a hotspot origin for the chain. The Pacific–Antarctic Ridge near the eastern end of the Foundation chain has a present day spreading rate of 94 mm/yr (DeMets et al., 1990). Spreading is asymmetric with the Antarctic plate being ~20% faster than the Pacific plate. For the last 20 m.y., the PAR has migrated towards the north west in the hotspot reference frame. This resulted in the progressive nearing of the ridge to the Foundation hotspot. At about 4 m.y. (Maia et al., 1999), the ridge and the hotspot started to interact. This influence resulted in a significant change in the chemistry of the basalts (Hémond and Devey, 1996; Devey et al., 1997), prompting a mixing between a HIMU source, attributed to the Foundation hotspot, and a MORB source, associated to the Pacific–Antarctic Ridge (Hémond and Devey, 1996). The progressive nearing of the ridge towards the hotspot over time also appears to have influenced the morphology of the edifices (Fig. 2). Volcanic morphology changes from individual edifices in the north west, to volcanoes grouped in ridges in the middle of the area and to smooth elongated ridges formed by coalesced calderas at the south-eastern end near the PAR axis. Such changes probably reflect the reduction in the elastic thickness of the lithosphere towards the PAR, the volcanoes being formed on a progressively younger plate (Maia et al., 1999).

The present location of the hotspot could not be pinpointed, since off-axis zero age lava flows were not observed. Lack of volcanic edifices on the east flank of the ridge however strongly suggests that the hotspot is still located beneath the Pacific plate, quite near the ridge axis (Devey et al., 1997). Such a near-axis location is compatible with the general age pattern of the Foundation chain (O'Connor et al., 1998). An analysis of the medium wavelength geoid reveals a ~15 cm amplitude positive anomaly centred over the North System (Fig. 2). This supports this idea and tentatively locates the hotspot beneath the elongated ridges near the PAR axis (Maia et al., 1999).

### 3. Data set and methodology

A full bathymetry coverage of the study area was obtained with a SIMRAD EM-12 dual multibeam echo-sounder. This echo sounder is composed of

two independent echo sounders each with 81 beams, adding up to 162 beams and with a ping repetition rate of 20 s. Precision is 2–3‰ of the water depth. The swath coverage depends on the aperture angle. During the cruise, a constant value of 150° allowed a coverage of 7.4 times the water depth. For most of the surveyed area, the track spacing allowed overlapping at the edges of the swaths, except above the shallowest volcano summits, where data gaps were unavoidable. In order to minimise these gaps, multibeam data from the RF *Sonne* survey of 1995 (Devey et al., 1997) are included in the final bathymetric grid. The Digital Elevation Model used for the study of the ridge morphology was computed with a 400 m grid spacing, using a near-neighbour algorithm (CARAIBES Software, IFREMER) (Fig. 2). A second bathymetric grid was computed with a continuous curvature gridding algorithm (GMT Software, Wessel and Smith, 1998) and a coarser grid interval (1.2 km) over 512 × 512 points and used for the gravity modelling. To fill the data gaps on the extremes of the grid, as required for Fourier analysis, we completed the data set with data available in the NOAA data bank as well as with data from the ETOPO5 world bathymetry grid. This minimises the spurious effects that might arise from extrapolation. The bathymetry for the area studied here is shown in Fig. 3a.

Gravity data were acquired with a Bodenseewerk KSS-30 gravity meter at a 10 s sampling rate and processed in the normal way: Eotvös and drift corrections, and removal of the WGRS80. Cross over errors were calculated for the data set. After cross-over error minimisation, the final data STD error is 1.2 mGal. The wide spacing of the profiles (7–8 miles, ~13–14 km) prevented the construction of a detailed ship-borne free air anomaly grid, so we used a merged satellite-ship free air anomaly grid (Sandwell and Smith, 1997) to obtain a MBA grid. In our case, merging is useful to both fill data gaps in the gravity coverage associated with the track spacing of the ship profiles (~28 km cross-track wavelength resolution) and reduce the directional artefacts that may arise from the regular orientation of the ship profiles. The ship data contain more short-wavelength information than the satellite data. In order to improve the merging of the two data sets we first calculated the difference between the satellite and ship free air data at each point along the profiles (Sandwell, personal

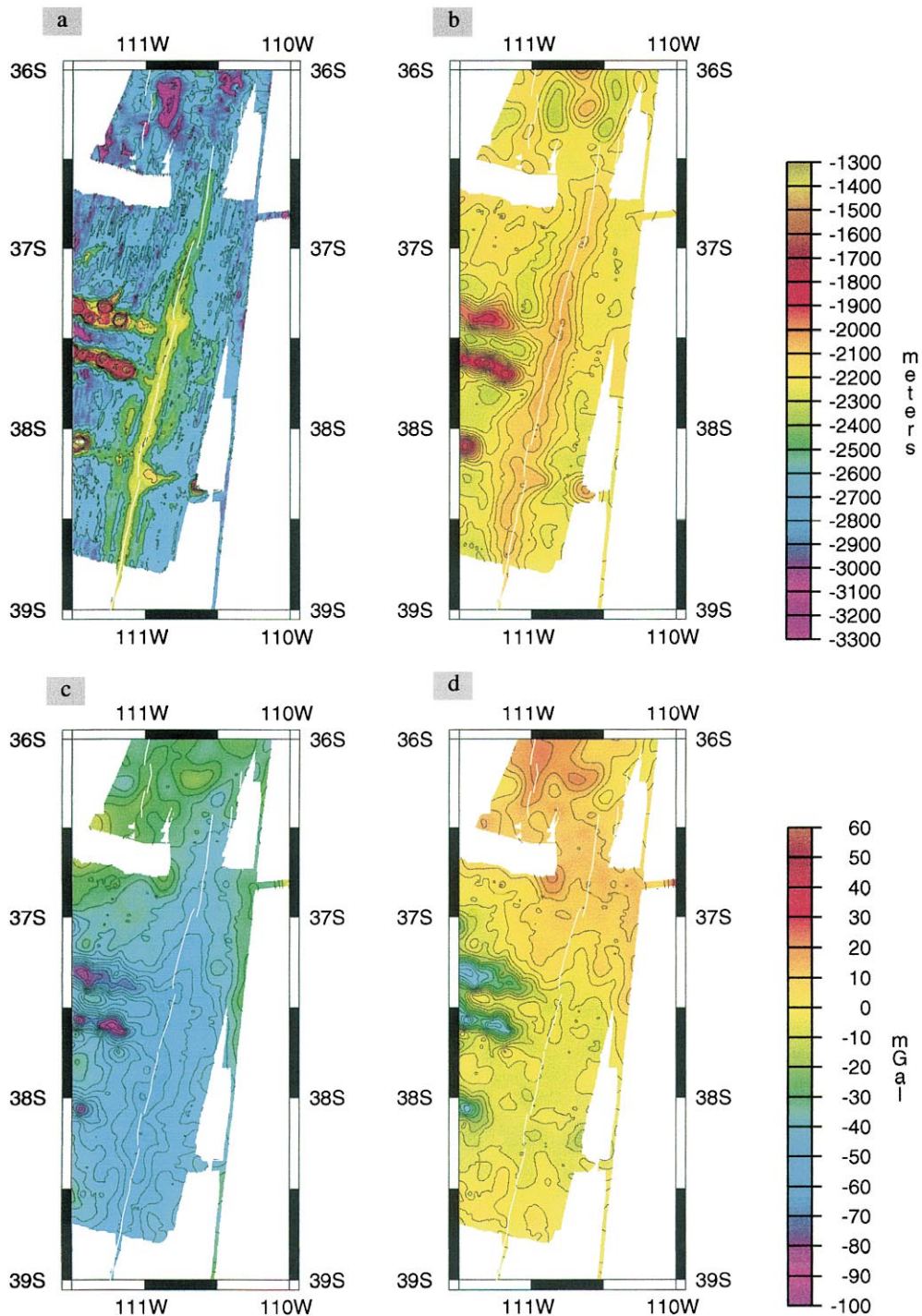
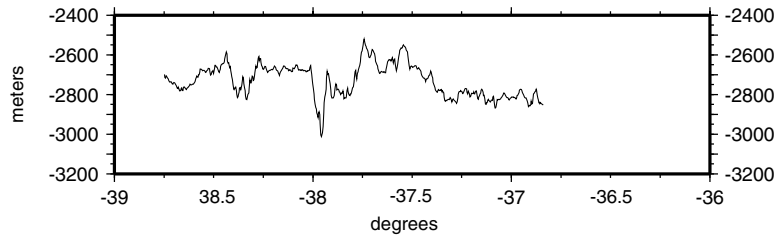
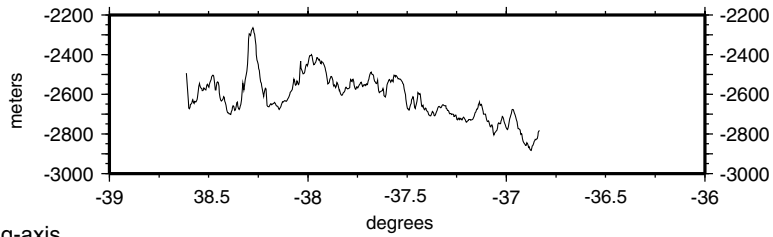


Fig. 3. (a) Multibeam bathymetry. (b) Merged ship-satellite free air anomaly. (c) Mantle Bouguer anomaly. (d) Residual Mantle Bouguer anomaly for the axial area of the Pacific Antarctic ridge.

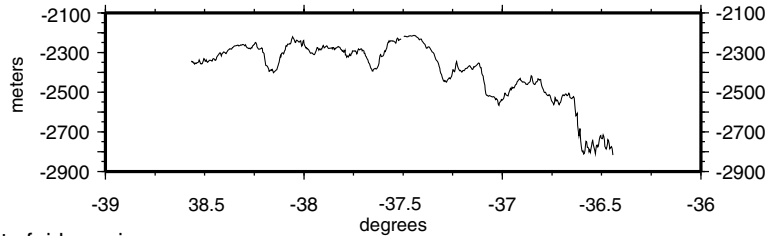
a East of ridge axis



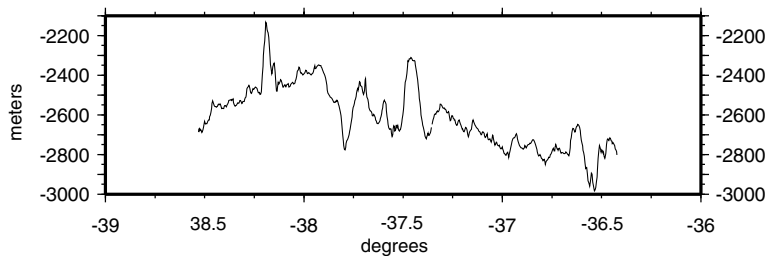
b



c Along-axis



d West of ridge axis



e

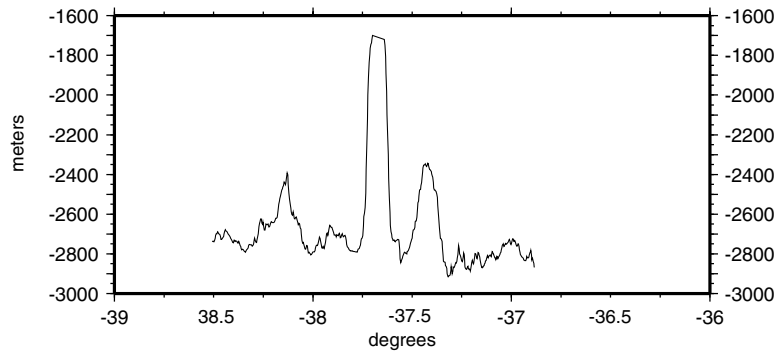


Fig. 4. Along-axis depth profiles. Profile locations are shown in Fig. 1. Depths are in meters. The axial profile is profile (c). Profiles (a) and (b) run on the Antarctic plate while profiles (d) and (e) run on the Pacific plate.

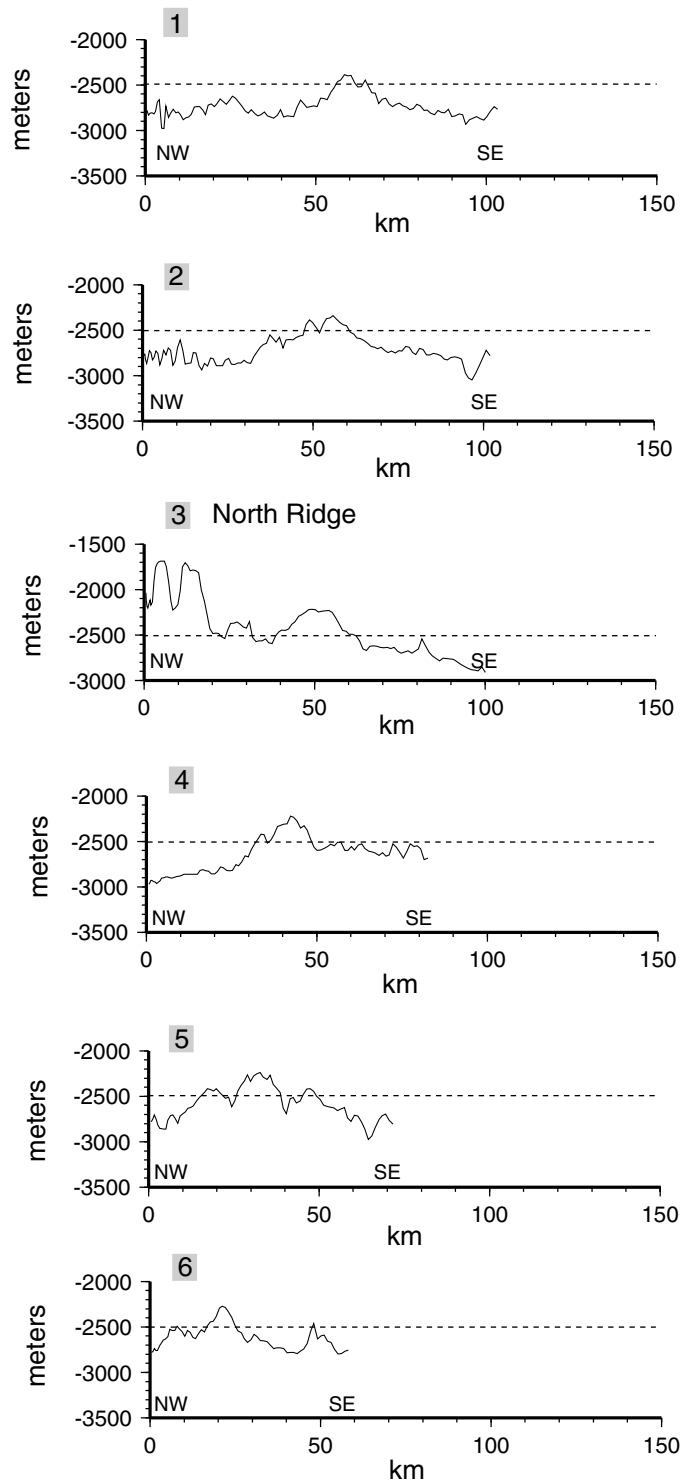


Fig. 5. Across-axis depth profiles. See Fig. 1 for location. Dashed line corresponds to the 2500 m depth. Distances in kilometres from the western end-point of the profiles.

communication). This difference was then gridded at a 1.2 km grid step and added to a satellite-only grid with the same grid spacing (Sandwell and Smith, 1997). This results in a smooth grid that also matches the ship gravity measurements. The continuous curvature gridding algorithm (Wessel and Smith, 1998) was used for the interpolation. The final grid for the axial area is shown in Fig. 3b.

#### **4. Morphology of the off-axis volcanoes of the ridge–hotspot interaction zone**

Petrology, basalt geochemistry (Hémond and Devey, 1996; Devey et al., 1997; Hékinian et al., 1997) and volcanic morphology define the ridge–hotspot interaction zone. This region (Fig. 2) extends 400 km away from the ridge axis and volcanism is scattered over a wide band. Volcanoes line up along two roughly parallel lines, separated by a distance that decreases towards the PAR, from ~150 km to less than 70 km. Near the PAR axis, the two lines almost merge to form three sub-parallel ridges, called North and South Ridges, for the northern line, and Planck for the southern line. A rough estimate of seamount volume for the northern line yields 2–3 times the volume of the southern line, suggesting that the northern system, that lies in the prolongation of the older Foundation volcanoes and where the geoid maximum is observed (Maia et al., 1999), is the main locus of volcanism.

The morphology of the edifices is variable. Average summit depths increase towards the PAR while the volume of the edifices decreases. The westernmost volcanoes are tall, well-formed circular or elongated edifices, sometimes displaying rift zones. Some of the tallest summits are flat and capped with carbonate reefs and sand, suggesting emersion or sub-surface depth in the past (Devey et al., 1997). Some of the large volcanoes are grouped into individual ridges. Further east, closer to the PAR axis, the edifices coalesce to form narrow ridges topped with calderas and bordered by steep scarps. Most of the orientations are oblique to the main trend of the Foundation seamounts. Small volcanic cones are scattered all over the area between the larger ridges. The lithospheric fabric, with elongated abyssal hills, parallel to the PAR axis, can be observed at several places

between the ridges. Crustal ages range from 8.9 m.y. in the west of the survey area to 0 m.y. Volcanic ages obtained from modelling of volcano magnetisation decrease to the east from 5 to near 0 m.y. (Maia et al., 1999) and the age of the lithosphere at the time the edifices were emplaced decreases progressively towards the PAR, which is compatible with the accreting centre approaching the hotspot. Radiometric ages for the volcanoes (O'Connor et al., 1998) agree with the ages derived from the magnetisation model.

#### **5. The Pacific–Antarctic Ridge axis: morphology and chemistry**

The PAR axis in the Foundation area is formed by a 500 km long segment limited by two large offset OSCs and disrupted by several minor discontinuities (Lonsdale, 1994). The axial area is broader and shallower than in the neighbouring segments (Lonsdale, 1994). The northern discontinuity, the 36.5°S OSC is a 45 km left-lateral OSC and represents the largest axial discontinuity of the PAR from the Juan Fernandez microplate to the Menard FZ, at 49.5°S. Lonsdale (1994) suggested that this offset has migrated southwards. The southern discontinuity, the 41.5°S OSC is a 27 km left-lateral OSC and is the second largest axial discontinuity within this province of the PAR. This OSC has migrated southwards, at least for the last 2 m.y., at a faster rate than the 36.5°S OSC, resulting in the lengthening of the Foundation PAR segment (Lonsdale, 1994).

Axial depths reach 2250 m where the off-axis volcanic ridges are closer to the axis (Figs. 3a, 4 and 5). A small amplitude (~200 m) along-axis undulation of the topography with a ~35 km wavelength, partially related to a second-order axial segmentation, exists. The largest and shallowest topography is related to the off-axis North Ridge (Fig. 4, profile c). The whole section of the PAR, where the three off-axis volcanic ridges approach the axis, displays a broad and shallow (~2250–2300 m) axial elevation (Fig. 5, profiles 3–6) and has the smooth morphology characteristic of fast spreading ridges. The volcanic ridges form a continuous feature with the PAR above the 2500 m isobath (Fig. 5, profiles 3 and 5). At these intersections, the PAR axis presents smooth, elevated circular areas, the largest being located near

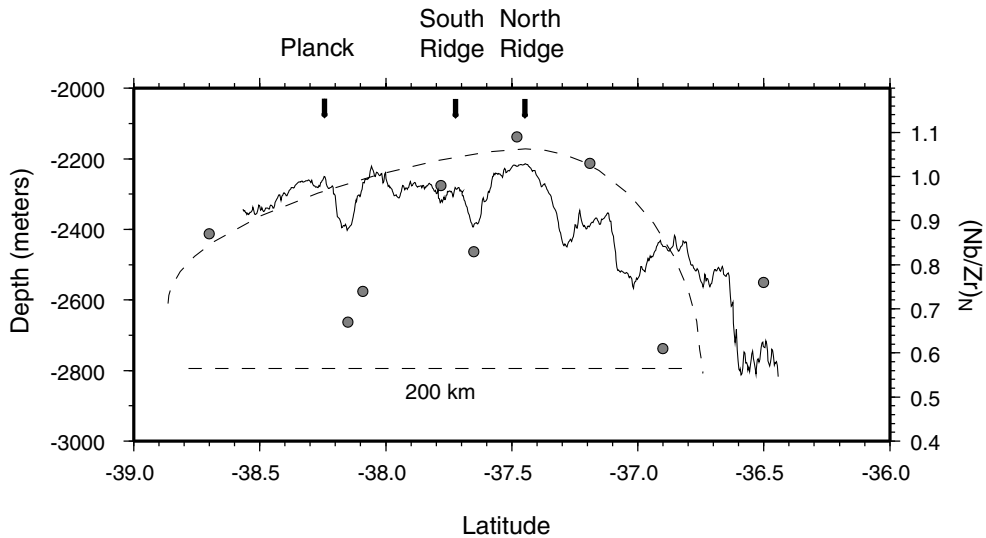


Fig. 6. Axial bathymetry (profile c) with values of  $(\text{Nb}/\text{Zr})_N$  ratios for the Pacific–Antarctic Ridge dredges. The two extreme dredges (north and south) were obtained during the Foundation Hotline cruise of L'Atalante. The other dredges are from Devey et al. (1997). Arrows show the emplacement of the off-axis volcanic ridges. The dashed curved line follows the trend of the chemical anomaly. The dashed line below the profile shows a scale for 200 km.

the North Ridge intersection. A bottom video camera profile taken over the axis at this location during the cruise showed flat lava surfaces and lava lakes, suggestive of high production rates. The morphology at these inflated points could be interpreted as very smooth and incipient volcanic cones. The axial morphology is highly suggestive of a focused magmatic production along relatively short (35–50 km) segments, closely related to the presence of off-axis volcanic features.

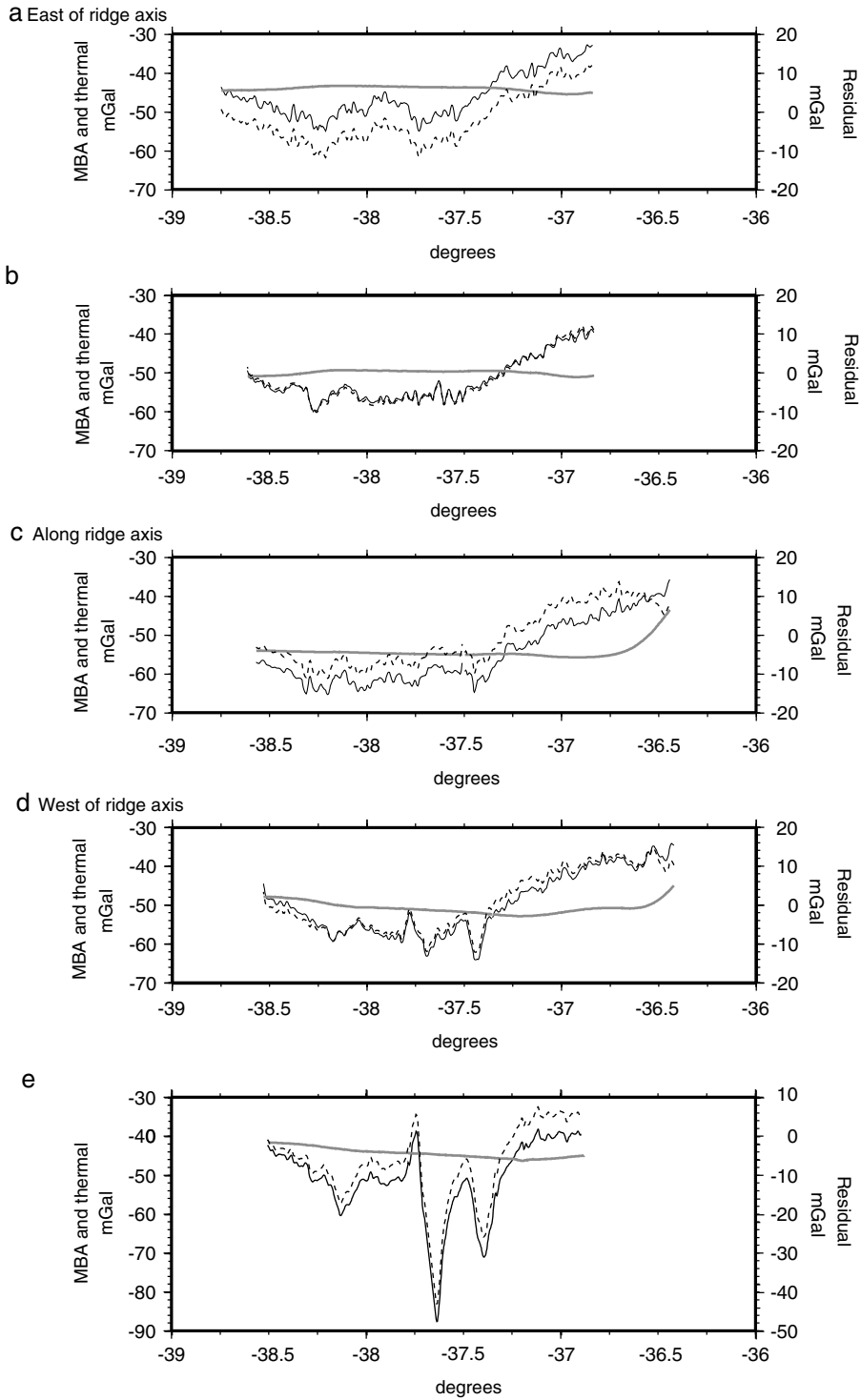
North of the Foundation seamounts, the PAR axis deepens (down to 2800 m) and narrows significantly when it approaches the 36.5°S OSC, south of the Juan Fernandez microplate (Lonsdale, 1994) (Fig. 4, profiles b–d and Fig. 5, profile 2). South of the Foundation seamounts, the ridge axis does not deepen and narrow as much (Figs. 3a and 4). Instead, we observe a flattening of the axial depth accompanied by a small decrease in the width of the axial elevation. According to Lonsdale's axial survey (Lonsdale, 1994), the aver-

age depth of the axial area remains fairly constant between 37.2°S and 39.5°S and decreases further south towards the 41.5°S OSC. This deepening never reaches, however, the gradients observed near the 36.5°S OSC.

On the east flank of the PAR, the lithospheric fabric near the ridge axis is undisturbed by volcanic features, with the exception of a single small off-axis volcano located 38°15'S. Rocks dredged from this volcano have a depleted MORB composition (Devey et al., 1997). Near this edifice, the axis broadens and forms a triangle-shaped plateau. No clear connection between the volcano and the axis, similar to those observed for the features on the west flank, is visible. Along the section facing the off-axis volcanic ridges of the west flank, the sea floor of the east flank is shallower and forms a wide elongated plateau (Fig. 3a).

The most enriched axial basalts were recovered where the North and South Ridges approach the

Fig. 7. Along-axis gravity profiles. See Fig. 1 for profile's location. The thin black line corresponds to MBA profiles, the dashed line to the Residual MBA profiles and light grey lines to the gravity effect of the thermal model. Scales on the left (in mGal) correspond to the MBA and to the thermal contribution. Scales on the right correspond to the residual anomaly.



PAR axis (Devey et al., 1997) (Fig. 6). Two dredges taken during our cruise (see inset of Fig. 1 for the location of these dredges) allow us to determine the extent of the hotspot influence along the axis. Devey et al. (1997) estimated this extent to be roughly 100 km. The northern dredge ( $36^{\circ}30'S$ ), although not showing the most depleted composition of the area, has a  $(Nb/Zr)_N$  ratio below 0.8. Our southern dredge, located at  $38^{\circ}40'S$ , on the contrary, has sampled basalts which show a higher value for the  $(Nb/Zr)_N$  ratio ( $(Nb/Zr)_N$  ratio above 0.8) (Hékinian et al., 1999) than the samples obtained at  $38^{\circ}10'S$  (Devey et al., 1997). The increase in the  $(Nb/Zr)_N$  ratio is however not strong enough to match the values observed near the supposed location of the hotspot, at  $37^{\circ}30'S$  (Fig. 6). These new data suggest that the chemical influence of the hotspot on the ridge may extend further south than previously thought. Lead isotopes (Hémond and Devey, 1996) confirm the influence of the neighbouring Foundation plume in the composition of the lavas at the PAR axis.

## 6. Gravity anomalies and crustal structure of the PAR axis

In order to address the problem of the crustal structure of the off-axis volcanic ridges and the relationship they may have with the axis of the Pacific–Antarctic Ridge, we calculated the Mantle Bouguer anomaly (MBA), a technique currently applied to mid-oceanic ridges studies (e.g. Prince and Forsyth, 1988; Pariso et al., 1995; Maia and Gente, 1998). In this model, crustal thickness is assumed to be constant (6 km) and the gravity effect of both the topography and the Moho interfaces are computed and removed from the free air anomaly. Densities are also held constant for both the crust and the mantle, respectively, 2700 and 3300 kg/m<sup>3</sup> (e.g. Kuo and Forsyth, 1988; Scheirer et al., 1998). Mantle Bouguer anomalies can be interpreted as deviations from the assumed model, either as crustal thickening or as lower crustal or mantle densities. The gravity effect of the model was computed using

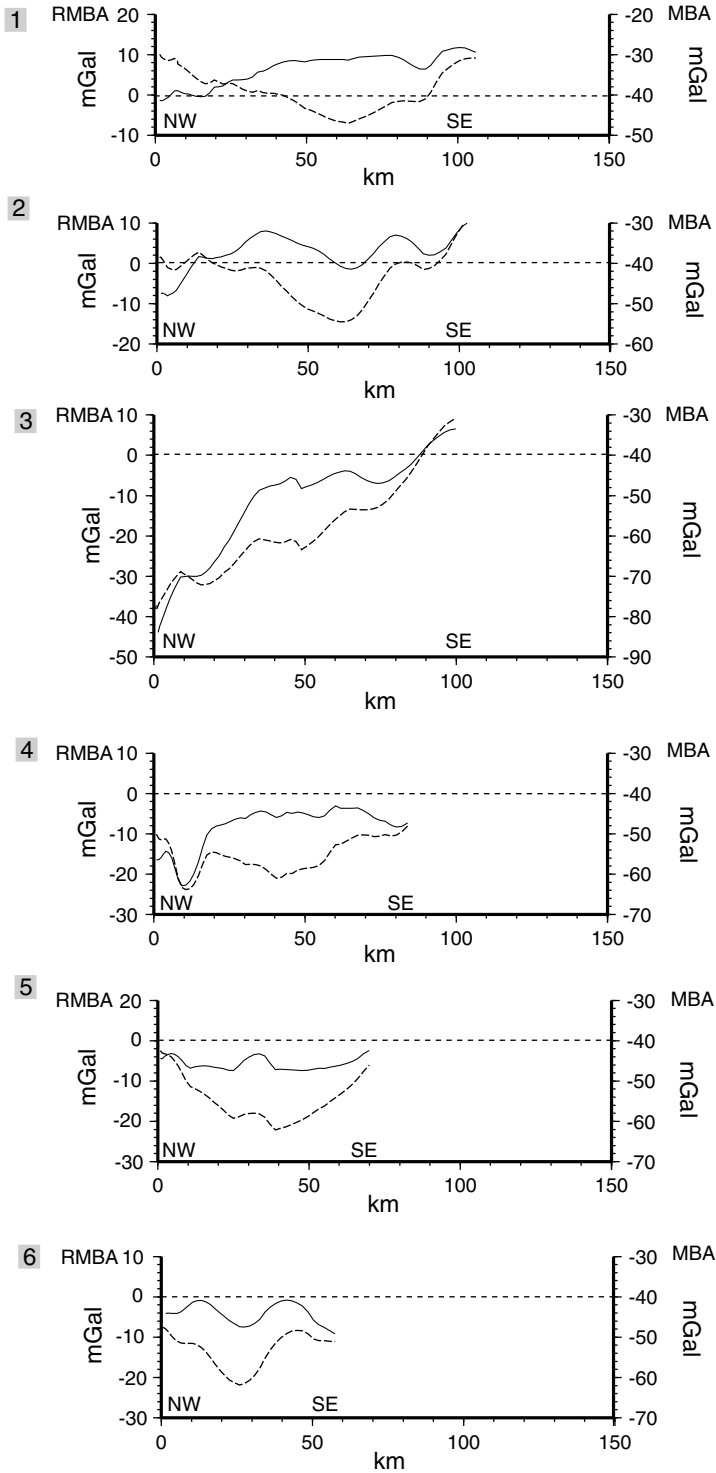
Parker's (1972) method in a fully three-dimensional way. The MBA is displayed in Fig. 3c.

The MBA map (Fig. 3c) and profiles (Figs. 7 and 8) show that the axial part of the PAR near the elongated volcanic ridges is characterised by a minimum in the MBA, well correlated with the wider axial section and shallower depths (Fig. 3a). The along-axis amplitude variation is of  $\sim 28$  mGal, with values ranging from  $-36$  mGal at the northern end of the ridge segment to  $-64$  mGal, near the elongated off-axis volcanic ridges (Fig. 7, profile c). Across-axis amplitudes vary from 18 mGal in the north to 47 mGal across the axis near the North Ridge and decrease to 21 mGal to the south (Fig. 8). On the profiles parallel to the ridge axis (Fig. 7), amplitude variations do not vary significantly between profile c (axis) and profiles a, b and d (off-axis) (amplitude variations of 22–24 mGal) with the exception of profile d, that crosses the volcanic ridges (amplitude variation of 50 mGal) and reflects the presence of crustal roots.

Mantle Bouguer Anomalies are dominated by the long wavelength signal related to lithosphere cooling away from the ridge axis. This causes the anomalies to be more negative at the axis. An along-axis thermal signal related to the presence of intermediate to large offset discontinuities also exists (Phipps Morgan and Forsyth, 1988). In order to remove from the MBA the signal related to both these processes, we calculated the gravity effect of a cooling lithosphere, using Phipps Morgan and Forsyth's (1988) passive flow model. We assumed a symmetric spreading with 94 mm/yr full rate (DeMets et al., 1990), although this corresponds to a simplification of the spreading geometry. Thermal parameters for the mantle were taken to be  $3.4 \times 10^{-5} \text{ K}^{-1}$  for the thermal expansion coefficient and  $10^{-6} \text{ m}^2 \text{ s}^{-1}$  for the lithosphere thermal diffusivity (e.g. Phipps Morgan and Forsyth, 1988; Sparks et al., 1993). Our model was computed with 16 layers of variable thickness down to a depth of 100 km. Top and bottom temperatures were assumed to be 0 and 1300°C, respectively. The residual anomaly is displayed in Fig. 3d.

Fig. 7 displays the gravity effect of a cooling

Fig. 8. Across-axis gravity profiles. See Fig. 1 for location. MBAs are shown by dashed lines and residual MBAs by continuous lines. Dashed line corresponds to the 0 mGal level (for the residual anomaly) and to the  $-40$  mGal level (for the MBA). Distances in kilometres from the western endpoint of the profiles.



lithosphere, computed from the thermal model of Phipps Morgan and Forsyth (1988). It can be seen that the effect of the 36.5°S OSC, although of a significant amplitude (11 mGal at the axis, profile c) is restricted to the immediate vicinity of the discontinuity (some tens of kilometres). The cold effect of the offset alone cannot therefore account for the strong amplitude variation of the MBA at the northern part of the segment. Away from the 36.5°S OSC, the gravity effect is rather flat, reflecting the absence of other significant axial discontinuities.

The residual anomaly map (Fig. 3d) shows a broad small amplitude minimum (–10 mGal) centred in the area where the MBA minimum is observed. Across-axis amplitudes vary from 14 mGal at the northern part of the segment, to 50 mGal near the North Ridge and to 7 mGal at the southern part of the segment (Fig. 8). Amplitudes are smaller than the MBA due to the removal of the cooling effect. As discussed in the previous paragraph, along-axis residual MBA variations (22–50 mGal) resemble those of the total MBA due to the “flat” behaviour of the thermal component of the gravity signal. Because the thermal effect of the OSC is restricted to the vicinity of the 36.5°S discontinuity, the northward gradient of the residual anomaly is still steeper than the southward gradient (Fig. 7).

The negative residual anomaly (Fig. 3d) extends to the east flank of the PAR. The long wavelength of the residual signal is shown in Fig. 9, where the profiles parallel to the ridge axis are filtered with a gaussian filter with a cut-off wavelength of 100 km. Both the width and the amplitude of the residual anomalies are relatively similar for the east flank profiles (a and b), the axial profile (c) and the nearest west flank profile (d). Profile (e), that crosses the off-axis volcanic ridges reflects the strong signal of the crustal roots. The relative constancy of the long wavelength signal suggests that the process responsible for this negative signal has been regularly active for several millions of years. If we interpret negative residuals as reflecting areas of thickened crust or of lower densities in the crust and mantle, this long wavelength anomaly may reflect the influence of the neighbouring Foundation hotspot on the crustal structure of the PAR. In this case, the crust in the area near the hotspot would be thicker and/or less dense than below neighbouring parts of the ridge, possibly with associated lower

mantle densities. Volumetric estimations for the off-axis volcanoes (Jordhal et al., 1999) show a progressive decrease in the volume of off-axis erupted lavas starting ~2 m.y. ago, which suggests that the PAR begun at that time to act as a drain to the hotspot melts.

Extreme negative values are observed beneath the elongated volcanic ridges, both in the MBA and in the residual anomaly, and certainly correspond to the important crustal thickening of the compensating roots (Fig. 3c and d). An along-axis undulation is visible in the MBA map as a series of elongated lows. These small (5–10 mGal) amplitude axial minima seem to correspond to the off-axis elongated volcanic ridges and, both for the North and the South Ridge a connection can be clearly seen in the gravity maps. Finally, another axial minimum near 38°S does not appear to be correlated to any near-axis topographic structure although in Fig. 2, a subdued line of small cones can be seen further away from the axis.

We inverted the residual anomaly for crustal thickness variations after downward continuing the signal to the average Moho depth and filtering to remove wavelengths below 25 km (Morris and Detrick, 1991). The average crustal thickening (Fig. 10) corresponding to the long wavelength signal reaches 1.5 km if the total along-axis variation is considered. The short wavelength small amplitude gravity undulations can be explained by local crustal thickening of ~1 km. These are of course upper bounds, since part of the gravity signal may also correspond to crust or mantle density variations.

Such values are significant for fast spreading ridges, where along-axis gravity anomalies and crustal thickness variations are usually small. As a comparison, along-axis variations of the MBA are of the order of 12 mGal over the MELT experiment area of the EPR, where off-axis volcanism suggest a hot mantle beneath the ridge (Scheirer et al., 1998). Smaller variations are observed over other parts of the EPR, for example, less than 5 mGal for the segments at 9° and 13°N (Madsen et al., 1990; Wang et al., 1996). The along-axis variation obtained for the PAR near the Foundation chain (28 mGal) are higher than those of the MELT segment (12 mGal), suggesting that the neighbouring hotspot contributed to significantly increase the axial crustal production. This 28 mGal along-axis amplitude of the MBA

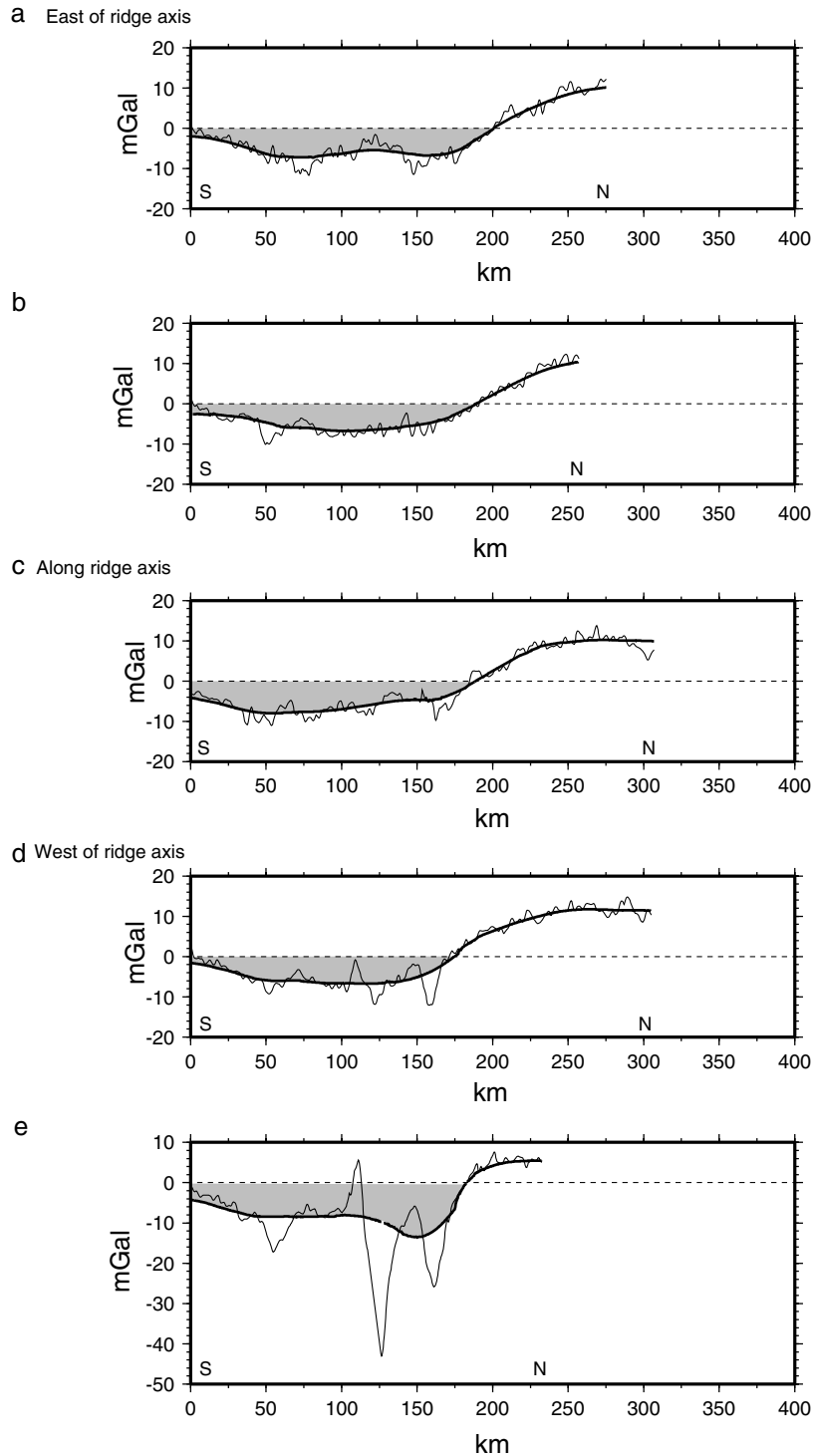


Fig. 9. Along-axis filtered residual MBAs. Grey shaded areas show the negative part of the signal. Profiles were projected in kilometres with an origin at their southern endpoint. The dimension of the shaded area is roughly equivalent for all the profiles.

remains smaller by one order of magnitude with respect to Galapagos, Easter, Iceland or Tristan ridge–hotspot systems (Ito and Lin, 1995a,b) where along-axis variations in the MBA may reach 340 mGal.

### 7. Comparison between the Foundation–PAR and other hotspot–ridge systems

As previously stated, available sampling does not allow to determine precisely the southern limit of the chemical influence of the Foundation hotspot. Devey et al. (1997) suggested a value of 100 km for the along-axis geochemical anomaly (**W**) but the new samples may indicate that some influence of the hotspot can be traced further south. The width of the chemical anomaly could be therefore increased at least to 200 km. Lack of along-axis sampling for the section of the PAR south of 39°S precludes determining precisely the extension of the along-axis chemical contamination. As the most enriched sample comes from locations near 37°24'S (Fig. 6), it can be assumed that the hotspot influence on the axis is the strongest at this latitude and declines away from it. The only available constraint for the southernmost extension of the chemical contamination of the Foundation hotspot along the PAR comes from samples described by Castillo et al. (1998) at 53°S showing very depleted basalts and no hotspot influence. We will adopt a 200 km conservative figure for **W**, based on our dredges but one must keep in mind that a larger value is also possible.

The along-axis flow of plume contaminated material away from the hotspot is not symmetric. Southward flow appears to extend further away from the supposed location of the hotspot than the northward flow. Gravity anomalies and inferred crustal thicknesses show a slight deviation to the south between the off-axis volcanic ridges and the PAR axis. Moreover, the axial depth of the ridge axis remains relatively constant as far as 39.5°S, then deepens gently towards the 41.5°S OSC (Lonsdale, 1994). This relatively flat topography could indicate that the along-axis flow still influences the ridge axis to 41.5°S OSC, although to a lower degree than near the Foundation seamounts. Such a southward flow could also contri-

bute to the fast migration rates observed for the 41.5°S OSC (Lonsdale, 1994). This asymmetric flow pattern agrees with the suggestion of Castillo et al. (1998) that in the South Pacific, the upper mantle may be flowing to the south-west.

In order to compare the Foundation hotspot–PAR system to other studied cases of ridge–hotspot interactions, we applied the relationships derived by Schilling (1985) for systems where a ridge is centred above or is moving away from a hotspot. The present location of the Foundation hotspot was estimated from the location of the maximum of the geoid anomaly (Maia et al., 1999), yielding a ridge–hotspot distance of 36 km. There is a certain amount of uncertainty in this value. Indeed, estimating the present day position of the hotspot using the ages of the volcanoes and published rotation poles yields uncertainties of more than 100 km, depending on the chosen pole. This is mainly because of irregularities in the age pattern due to lithospheric control (O'Connor et al., 1998; Maia et al., 1999). Assuming that the positive geoid anomaly marks the present location of the hotspot, we are able to conveniently reproduce the age pattern of the chain by reconstructing its position backwards in time. The maximum of the geoid anomaly is located ~36 km west of the ridge axis and the swell is roughly 200 km wide. Since plumes are probably relatively wide, we added to this distance estimate an error bar of 150 km, corresponding to currently accepted plume diameters (e.g. Ito et al., 1997; Wolfe et al., 1997). **W**, as mentioned, was taken to be 200 km. The anomalous axial topography,  $\Delta E$ , was calculated using the same reference depth (2900 m) as used by Schilling (1985), which is deeper than the global average of ridge segments given by more recent models (Carlson and Johnson, 1994). We obtained a maximum value of 650 m for  $\Delta E$  (average  $630 \pm 100$  m). Fig. 11 plots the values estimated for **W** and  $\Delta E$  for the Foundation–PAR system as a function of ridge–hotspot distance, compared to the results of Schilling (1985). The Sala y Gomez–Easter estimation of Schilling (1991) was added to the plot. We did not however include the points for the Indian Ocean hotspots of Schilling (1991). Recent data indeed suggests that, at least for Kerguelen–Amsterdam (Graham et al., 1999) and Reunion (Dyment, personal communication), the history of their interaction with the nearest spreading ridge may be complex. The Foundation–PAR system

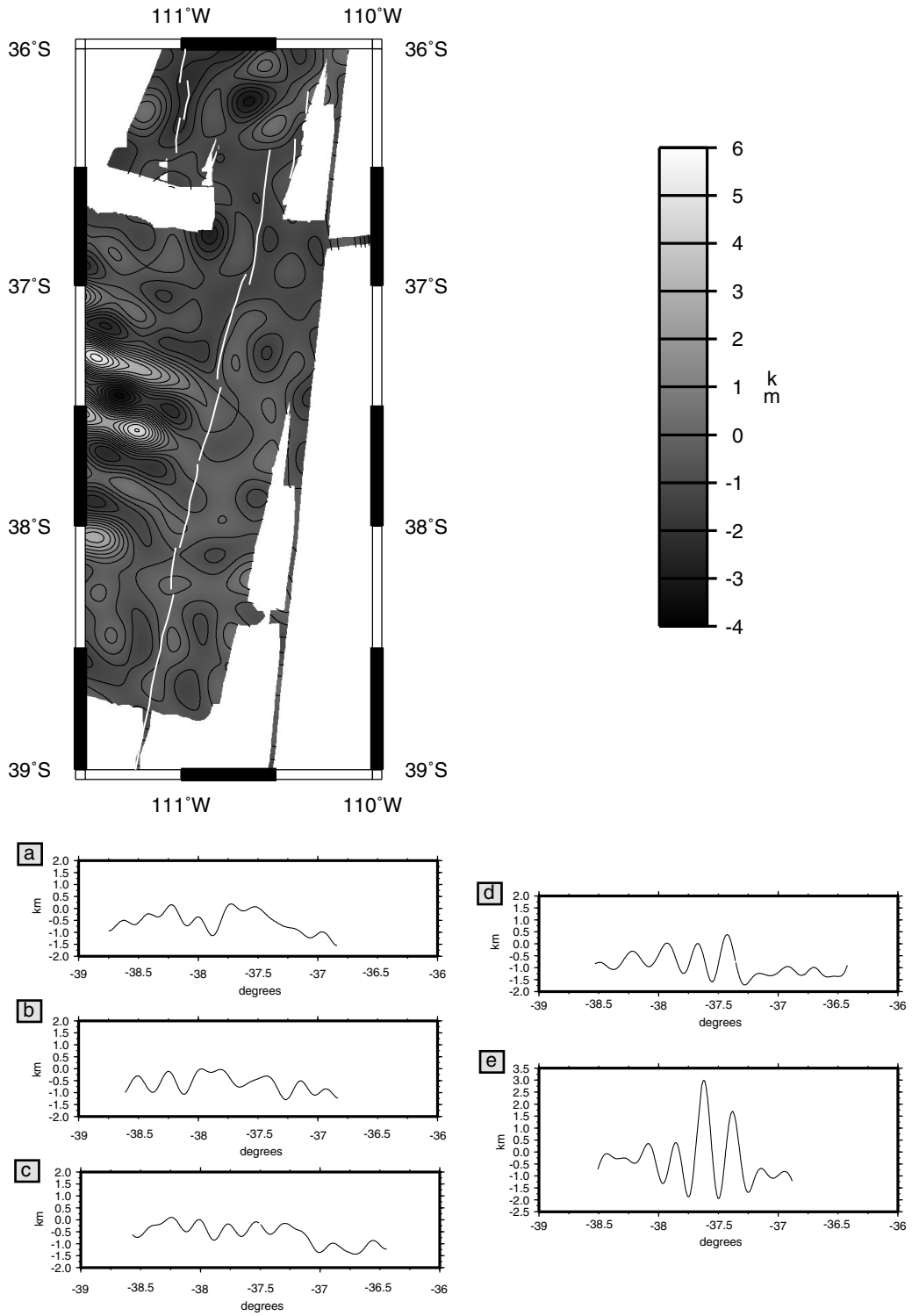


Fig. 10. Crustal thickness variations (in kilometres) over the axial area and along profiles. The white line on the map follows the PAR axis.

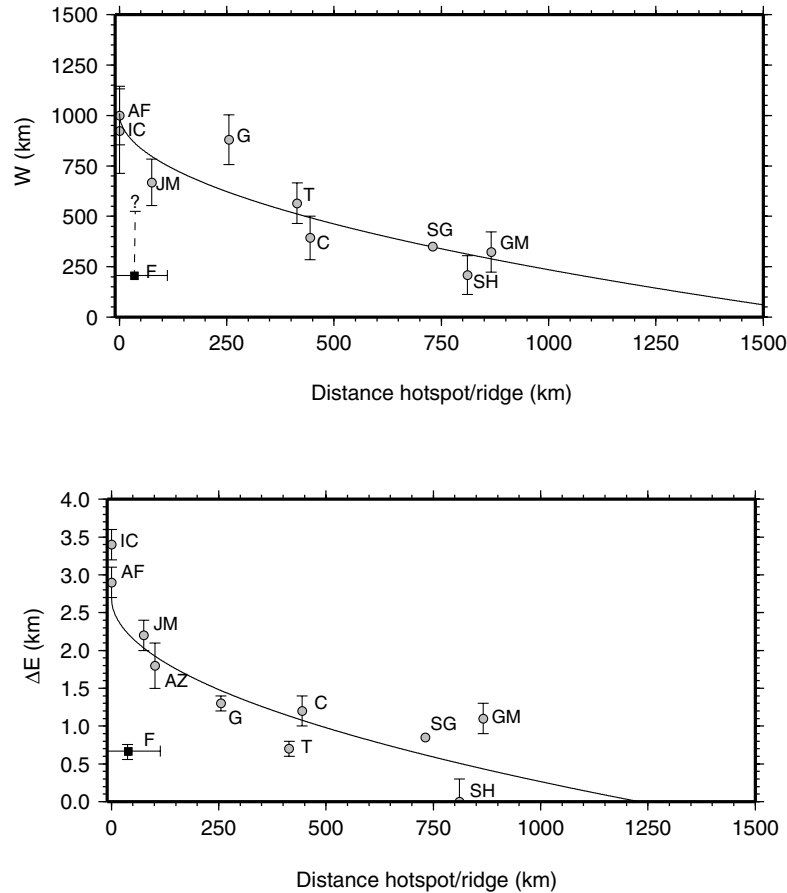


Fig. 11. Plots of the relationship between the ridge–hotspot distance and the width of the chemical anomaly ( $W$ ) and between the ridge–hotspot distance and the anomalous axial elevation ( $\Delta E$ ). Grey circles are values from Schilling (1985, 1991) and the black square corresponds to the values for the Foundation–PAR system (this paper). The theoretical laws derived by Schilling (1985) are indicated by thin lines. Error bars for the Foundation estimates are explained in the text. The following hotspots are represented: Iceland (IC), Afar (AF), Foundation (F), Jan Mayen (JM), Azores, (AZ), Galapagos (G), Tristan (T), Circe (C), Sala y Gomez (SG), St. Helena (SH) and Great Meteor (GM).

clearly departs from the empirical law derived by Schilling and falls much below the predicted values for both parameters. For a ridge–hotspot distance of 36 km, along-axis extension of the chemical contamination ( $W$ ) should be 860 km and the anomalous axial elevation ( $\Delta E$ ) 2150 m, more than three times greater than the values obtained in the present study. While there is some indetermination in the definition of the along-axis chemical anomaly ( $W$ ), the anomalous elevation ( $\Delta E$ ) is well constrained. Values as high as the predicted ones for  $\Delta E$  would result in axial depths of  $\sim 700$  m, almost as high as some of the off-axis volcanoes! The chemical contamination could extend further south. The along-axis distance

between the hotspot and the  $41.5^\circ\text{S}$  OSC is less than 500 km but axial discontinuities are not necessarily barriers to the mantle flow. In order to reach the 860 km predicted value, the chemical influence of the Foundation hotspot should extend down to  $\sim 46^\circ\text{S}$ .

Comparison of the predicted and observed ridge excess elevations and of the less constrained extension of the chemical contamination suggest that in the case of a fast ridge approaching a hotspot, the relationship derived for other studied systems may not hold. Clearly, the amount of plume material reaching the ridge axis is smaller. The rather low values obtained for the along-axis MBA variation, compared to those obtained for other ridge–hotspot systems (Ito and Lin,

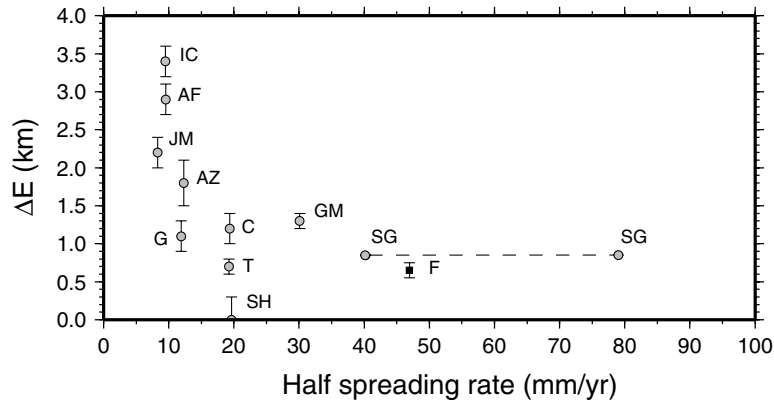


Fig. 12. Relationship between spreading rate and ridge anomalous elevation related to hotspots  $\Delta E$ . Grey circles are values from Schilling (1985, 1991) and the black square correspond to the Foundation–PAR system (this paper). The two points for Sala y Gomez (SG) are plotted for spreading rates of 80 mm/yr (Schilling, 1991) and 158 mm/yr (Ribe and Delattre, 1998). This difference arises from whether one considers the spreading rate at the East Ridge of the Easter microplate as being half the total rate of the EPR (Schilling) or as being the total rate (Ribe and Delattre).

1995a,b) reinforces the idea that, for the Foundation–PAR system, an interaction process different from the channelled laminar flow may be active. Three factors may contribute to generate these differences: (1) the fast spreading rate of the PAR; (2) the relative motion between the PAR and the hotspot; and (3) the magnitude of the plume volume flux.

It has been shown by different studies (Feighner and Richards, 1995; Ribe, 1996; Ito et al., 1997; Ribe and Delattre, 1998) that the along axis width of the plume contamination scales with  $(Q/U)^{1/2}$ , where  $Q$  is the plume volume flux and  $U$  the ridge spreading rate. High spreading rates will therefore contribute to reduce the plume flux directed towards the ridge (Kincaid et al., 1996; Ribe, 1996; Ribe and Delattre, 1998). This is coherent with the observation that the anomalous axial elevation  $\Delta E$  and the along-axis extension of the topographic anomaly are inversely proportional to the spreading rate (Vogt, 1976; Schilling, 1985; Ito and Lin, 1995b). The  $\Delta E$  values obtained for the Foundation–PAR system are coherent with such a trend (Fig. 12).

Relative plume–ridge migration will considerably influence the dynamics of the interaction (Ribe, 1996; Ito et al., 1997; Ribe and Delattre, 1998). The relative movement of a ridge approaching a hotspot, especially at rates comparable to the half-spreading rate (which is the case of the Foundation–PAR system) will contribute to reduce the plume–ridge flow

(Ribe, 1996; Ito et al., 1997; Ribe and Delattre, 1998). Ito et al. (1997) and Ribe and Delattre (1998) showed that, in the case of a ridge approaching a plume, the plate leading the ridge will move faster with respect to the plume. The additional speed induces more drag on the plume away from the ridge, therefore hindering and delaying the interaction. On the contrary, the distances at which the connection remains active will be greater for the cases where a ridge is moving away from a plume, because the plate trailing the ridge will move slower. The effect of the ridge–hotspot relative movement is larger for fast ridge–hotspot migration velocities.

The amount of plume material reaching the ridge also depends on the plume–ridge distance, on the plume temperature and viscosity and on the slope of the base of the lithosphere (Ribe, 1996; Ito et al., 1997; Ribe and Delattre, 1998). Plume viscosity and temperature appear to have only a minor influence on the dynamics of plume–ridge interaction (Ito et al., 1997; Ribe and Delattre, 1998). Kincaid et al. (1995, 1996) suggested that the slope of the base of the lithospheric plate is essential for the establishment of a flow towards the ridge. However, results from Ito et al. (1997) and Ribe and Delattre (1998) show that this is a second-order effect on the dynamics of the interaction because of the accretion of plume material to the base of the lithosphere. While the upslope flow tends to enhance the interaction, accretion of plume

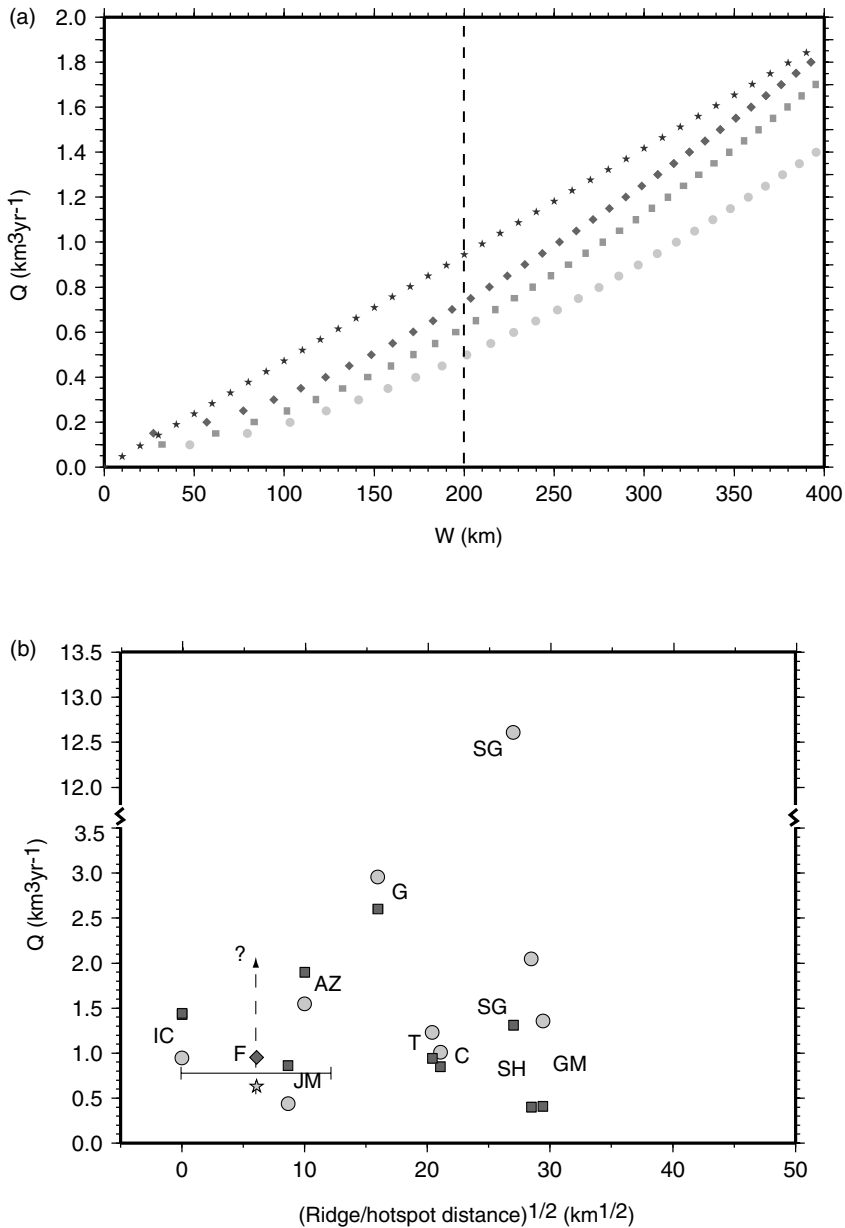


Fig. 13. (a) Estimates of plume volume flux ( $Q$ ) for the Foundation hotspot as a function of the along-axis width of plume contamination ( $W$ ). The  $Q$  values were computed using Schilling (1991) (black stars), Ito et al. (1997) (dark grey diamonds), Ribe and Delattre (1998) (medium grey squares) and Ribe (1996) (light grey circles) models. For a given  $W$ , the smallest  $Q$  values are obtained for Ribe (1996) fixed ridge model, showing that a ridge migrating towards a hotspot (Ito et al., 1997; Ribe and Delattre, 1998) reduces the amount of plume material reaching the ridge axis. (b) Relationship between hotspot volume fluxes ( $Q$ ) and ridge-hotspot distance for different plumes: Iceland (IC), Foundation (F), Jan Mayen (JM), Azores, (AZ), Galapagos (G), Tristan (T), Circe (C), Sala y Gomez (SG), St. Helena (SH) and Great Meteor (GM). Light grey circles are from Ribe and Delattre (1998) and medium grey squares are from Schilling (1991). No error bars were represented for these estimates on purpose. The large difference on the Sala y Gomez estimates (note the interruption in the vertical axis) arise from the different spreading rates considered by Schilling (80 mm/yr) and by Ribe and Delattre (158 mm/yr) in their calculations. The light grey stars and the medium grey diamonds correspond to values derived for the Foundation-PAR system (this paper) using Ribe and Delattre (1998) and Schilling (1991) models, respectively. The vertical arrow indicates that higher values for  $Q$  may correspond to larger along-axis contamination distances ( $W$ ).

material tends to decrease it. For plumes located near the ridge axis, where the slope of the base of the plate is the steepest, the upslope flow effect is greater than for plumes located far away, remaining however small.

Morgan (1978) and Schilling (1985, 1991) suggested that the efficiency of the channelling between a plume and a spreading ridge might be increased by the formation of a narrow thermal groove at the base of the lithosphere. However, different models showed that the effect of lithospheric erosion, although enhancing the flow, is minor (Kincaid et al., 1995, 1996; Ito et al., 1997; Ribe and Delattre, 1998). Moreover, such a narrow channel might be created only in the case of a ridge moving away from a hotspot (Ribe, 1996).

The departure of the Foundation–PAR system from the predicted relationship of Schilling (1985) implies a smaller amount of plume material reaching the ridge axis. Therefore, quantifying the volume flux  $Q$  and excess temperature at the ridge axis for the Foundation plume with the method developed by Schilling (1991), where most of the plume material is assumed to reach the ridge axis, is hazardous. However, this method can place some bounds on the parameters of anomalous elevation and along-axis width of the plume contamination. Volume flux estimates were also computed using the scaling laws published by Ito et al. (1997) and Ribe and Delattre (1998). These recent models have the advantage of including the realistic case of a migrating ridge, but their disadvantage is that volume fluxes are estimated based on the observed  $W$ , which in our case is only poorly constrained. A comparison of the plume volume fluxes obtained using these different models is shown in Fig. 13a for  $W$  ranging from 0 to 400 km. Values of 200°C and  $2.4 \times 10^{18}$  Pa s were adopted for plume temperature and viscosity (Ribe and Delattre, 1998) and an isoviscous case was used for the Ito et al. (1997) model so that comparisons with Ribe and Delattre (1998) are simplified. Values of  $Q$  for the case of a stationary ridge (Ribe, 1996) are also shown. Schilling's method estimates are always higher than those obtained with the other models. Migrating ridge estimates for plume volume fluxes are higher than those for a stationary ridge for a given  $W$ , illustrating the weaker plume–ridge flow. Changing the plume temperature or viscosity will only slightly alter  $Q$  (Ribe and Delattre, 1998). As

an example,  $Q$  values for a 200 km along-axis width  $W$ , will range between 0.65 km<sup>3</sup>/yr for 200°C to 0.84 km<sup>3</sup>/yr for 50°C, using Ribe and Delattre's scaling laws. In Fig. 13b we plotted  $Q$  estimates for different plumes taken from Schilling (1991) and from Ribe and Delattre (1998) compared to our results for the Foundation plume. If we consider Ribe and Delattre's estimates as being the more realistic ones, the Foundation is one of the weakest plumes in terms of volume flux. These values are not inconsistent with the volume of magmatism produced by the plume. The Foundation hotspot indeed never produced volcanic edifices whose dimensions are comparable to other Pacific plate hotspots, such as Society, Austral or Hawaii.

As a last point in our comparison of the Foundation–PAR with other ridge–hotspot systems, we attempted to compute the temperature anomaly produced at the ridge axis by the plume. We adopted here the relationship derived by Ito and Lin (1995b) for five ridge–plume systems, although all of them consist of a ridge moving away from a hotspot. In order to do the comparison, we recalculated the  $\Delta E$  given by Schilling (1985, 1991) using a different reference depth of 2.6 km (Carlson and Johnson, 1994) to be compatible with Ito and Lin (1995b). The results are plotted in Fig. 14. Temperature estimates for the Foundation were also derived from the along-axis amplitude variation of the MBA, also following Ito and Lin (1995b), and both estimates were comparable (17°C for the MBA-derived temperature estimate compared with 16°C for the  $\Delta E$ -derived temperature estimate). Again, the Foundation–PAR system lies much below the temperatures of other ridge–hotspot systems. As an example, we can consider Jan Mayen, that is located at a comparable distance from the ridge and has a volume flux of the same order when compared to Foundation. Values of  $\Delta E$ ,  $W$  and  $\Delta T$  are much higher for Jan Mayen. This strongly suggests that the empirical relationships derived for ridge-centred systems or for systems where a ridge is moving away from the plume do not hold for the case where a ridge migrates towards the plume because a smaller amount of plume material is being channelled towards the ridge axis in the latter case. An alternative explanation for the low ridge axis anomalies is that the Foundation plume may be dwindling and becoming weaker. The

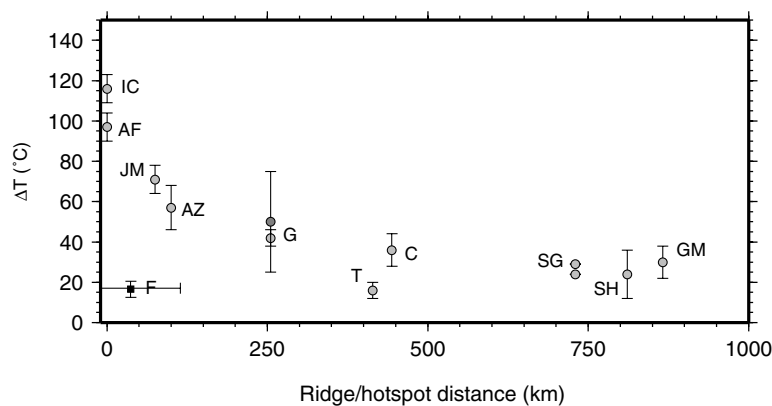


Fig. 14. Excess temperature at the ridge axis ( $\Delta T$ ) plotted as a function of ridge–hotspot distance, calculated using Ito and Lin (1995b) relationship, as explained in the text. Grey circles show values obtained for plumes using the  $\Delta E$  estimates from Schilling (1985, 1991) recalculated with a new reference depth of 2.6 km. Iceland (IC), Afar (AF), Jan Mayen (JM), Azores, (AZ), Galapagos (G), Tristan (T), Circe (C), Sala y Gomez (SG), St. Helena (SH) and Great Meteor (GM). The black square (F) correspond to values derived for the Foundation–PAR system (this paper). We included the  $\Delta T$  estimate of Ito and Lin (1995a) for the Galapagos hotspot (medium grey circle). The two estimates for the Sala y Gomez hotspot were calculated using two different spreading rates, 80 and 158 mm/yr.

geochemistry, morphology (Hémond et al., 1999; Maia et al., 1999) and age pattern (O'Connor et al., 1998) of the Foundation chain strongly supports a hotspot origin for the volcanoes. Moreover, the chemical pattern observed at the off-axis volcanoes near the PAR points to a dilution of the plume signature (Hémond et al., 1999), as reported for other ridge–hotspot systems (Haase et al., 1996; Kingsley and Schilling, 1998; Pan and Batiza, 1998). However, if the Ngatemato and Taukina ridges on the Austral chain are linked to the Foundation hotspot as suggested by McNutt et al. (1997) and O'Connor et al. (1998), the Foundation may be a plume presenting strong temporal variations in its volume flux, because no significant volcanic features can be seen between the Austral chain and the oldest volcanoes of the Foundation Seamounts. The volume flux estimates obtained in this paper however suggests that the Foundation plume, although relatively weak, is comparable to Jan Mayen in terms of  $Q$  and that the differences in the axial parameters observed for these two hotspots may be at least partly due to the different relative movements between the migrating ridge and the hotspot.

## 8. Conclusions

Along-axis analysis of the topography and gravity

anomalies (MBA and Residual MBA) for the segment of the Pacific–Antarctic Ridge near the location of the Foundation hotspot show evidence of ridge–hotspot interaction. The axial depths are shallower than in the neighbouring segments of the PAR and the gravity anomalies allow to infer crustal thickening and/or low crust and mantle densities. The chemical composition of the axial basalts confirm the existence of exchanges between the accreting ridge and the neighbouring hotspot.

A comparison of the along-axis MBA amplitude, anomalous axial elevation and extension of the chemical anomaly with results obtained for other ridge–hotspot systems, strongly suggests that the case of a fast spreading ridge that approaches a hotspot results in a weaker connection between the hotspot and the ridge axis. This is consistent with results of recent numerical models for the interaction between a migrating ridge and a hotspot.

## Acknowledgements

This study was funded by INSU-CNRS program “Intérieur de la Terre”, grant 97N51/0349. The “Foundation Hotline” cruise was supported by INSU-CNRS. The participation to the cruise of the German scientific team (P. Stoffers, D. Ackermann,

J. O'Connor, A. Dehghani and A. Sabetian) was funded by BMFB, Germany, as part of the French–German co-operation program for the study of the South Pacific volcanism. On board data treatment was performed using software developed by IFREMER. We thank Captain Gourmelon and his crew as well as the technical team from GENAVIR/IFREMER for their invaluable help during the cruise. Jean Goslin, Rodey Batiza, Garrett Ito and Hervé Chamley made careful reviews that considerably improved the quality of this paper. All figures were drawn using the GMT Software (Wessel and Smith, 1998).

## References

- Carlson, R.L., Johnson, H.P., 1994. On modeling the thermal evolution of the oceanic upper mantle: an assessment of the cooling plate model. *J. Geophys. Res.* 99, 3201–3214.
- Castillo, P.R., Natland, J.H., Niu, Y., Lonsdale, P.F., 1998. Sr, Nd and Pb isotopic variation along the Pacific–Antarctic rise crest, 53–57°S: implications for the composition and dynamics of the South Pacific upper mantle. *Earth Planet. Sci. Lett.* 154, 109–125.
- DeMets, C., Gordon, R.G., Argus, D.F., Stein, S., 1990. Current plate motions. *Geophys. J. Int.* 101, 425–478.
- Devey, C.W., Hékinian, R., Ackermann, D., Binard, N., Francke, B., Hémond, C., Kapsimalis, V., Lorenc, S., Maia, M., Möller, H., Perrot, K., Pracht, J., Rogers, T., Statteger, K., Steinke, S., Victor, P., 1997. The Foundation Seamount Chain: a first survey and sampling. *Mar. Geol.* 137, 191–200.
- Feighner, M.A., Richards, M.A., 1995. The fluid dynamics of plume–ridge and plume–plate interactions: an experimental investigation. *Earth Planet. Sci. Lett.* 129, 171–182.
- Géli, L., Aslanian, D., Olivet, J.-L., Vlastelic, I., Dosso, L., Guillou, H., Bougault, H., 1998. Location of Louisville hotspot and origin of Hollister Ridge: geophysical constraints. *Earth Planet. Sci. Lett.* 164, 31–40.
- Graham, D.W., Johnson, K.T.M., Douglas Priebe, L., Lupton, J.E., 1999. Hotspot–ridge interaction along the Southeast Indian Ridge near Amsterdam and St Paul islands: helium isotope evidence. *Earth Planet. Sci. Lett.* 167, 297–310.
- Haase, K., Devey, C.W., Goldstein, S.L., 1996. Two-way exchange between the Easter mantle plume and the Easter microplate spreading axis. *Nature* 382, 344–346.
- Hanan, B.B., Kingsley, R.H., Schilling, J.-G., 1985. Pb isotope evidence in the South Atlantic for migrating ridge–hotspot interactions. *Nature* 322, 137–144.
- Hékinian, R., Stoffers, P., Devey, C.W., Ackermann, D., Hémond, C., O'Connor, J., Binard, N., Maia, M., 1997. Intraplate versus oceanic ridge volcanism on the Pacific Antarctic Ridge near 37°S–111°W. *J. Geophys. Res.* 102, 12 265–12 286.
- Hékinian, R., Stoffers, P., Ackermann, D., Révillon, S., Maia, M., Bohn, M., 1999. Ridge–hotspot interactions: the Pacific–Antarctic Ridge and the Foundation Seamounts. *Mar. Geol.* 160, 199–223.
- Hémond, C., Devey, C.W., 1996. The Foundation Seamount Chain, Southeast Pacific: first isotopic evidence of a newly discovered hotspot track. *J. Conf. Abstr. (Goldschmidt, Heidelberg)*, vol. 1, p. 255.
- Hémond, C., Maia, M., Gente, P., 1999. The Foundation Seamounts: past and present ridge–hotspot interactions?. *EOS Trans. AGU* 80, 46 (Fall Meeting Suppl., F1056).
- Ito, G., Lin, J., 1995. Mantle temperature anomalies along the present and paleoaxes of the Galapagos spreading center as inferred from gravity analyses. *J. Geophys. Res.* 100, 3733–3745.
- Ito, G., Lin, J., 1995. Oceanic spreading center–hotspot interactions: constraints from along-isochron bathymetric and gravity anomalies. *Geology* 23, 657–660.
- Ito, G., Lin, J., Gable, C.W., 1997. Interaction of mantle plumes and migrating mid-ocean ridges: implications for the Galapagos plume–ridge system. *J. Geophys. Res.* 102, 15 403–15 417.
- Jordhal, K., Maia, M., Francheteau, J., 1999. The morphology of the Foundation Seamounts. *EOS Trans. AGU* 80, 46 (Fall Meeting Suppl., F1056).
- Kincaid, C., Ito, G., Gable, C., 1995. Laboratory investigation of the interaction of off-axis mantle plumes and spreading centres. *Nature* 376, 758–761.
- Kincaid, C., Schilling, J.G., Gable, C., 1996. The dynamics of off-axis plume–ridge interaction in the uppermost mantle. *Earth Planet. Sci. Lett.* 137, 29–43.
- Kingsley, R.H., Schilling, J.-G., 1998. Plume–ridge interaction in the Easter-Sala y Gomez seamount chain–Easter Microplate system: Pb isotope evidence. *J. Geophys. Res.* 103, 24 159–24 177.
- Kuo, B.-Y., Forsyth, D.W., 1988. Gravity anomalies of the ridge-transform system in the South Atlantic between 31 and 34.5°S: upwelling centers and variations in crustal thickness. *Mar. Geophys. Res.* 10, 205–232.
- Lonsdale, P., 1994. Geomorphology and structural segmentation of the crest of the southern (Pacific–Antarctic) East Pacific Rise. *J. Geophys. Res.* 99, 4683–4702.
- Madsen, J.A., Detrick, R.S., Mutter, J.C., Buhl, P., Orcutt, J.C., 1990. A two and three dimensional analysis of gravity anomalies associated with the East Pacific Rise at 9°N and 13°N. *J. Geophys. Res.* 95, 4967–4987.
- Maia, M., Gente, P., 1998. Three-dimensional gravity and bathymetry analysis of the Mid-Atlantic Ridge between 20°N and 24°N: flow geometry and temporal evolution of the segmentation. *J. Geophys. Res.* 103, 951–974.
- Maia, M., Dyment, J., Gente, P., Jouannetaud, D., 1999. The Foundation hotspot–Pacific–Antarctic ridge interaction: complexities of the channelling model revealed. *J. Conf. Abst. (EUG 10)*, vol. 4, p. 345.
- Mammerickx, J., 1992. The Foundation Seamounts: tectonic setting of a newly discovered seamount chain in the South Pacific. *Earth Planet. Sci. Lett.* 113, 293–306.
- Morgan, W.J., 1978. Rodriguez, Darwin, Amsterdam...a second type of hotspot island. *J. Geophys. Res.* 85, 5355–5360.

- Morris, E., Detrick, R.S., 1991. Three dimensional analysis of gravity anomalies in the MARK area, Mid-Atlantic ridge, 23°N. *J. Geophys. Res.* 96, 4355–4366.
- O'Connor, J., Stoffers, P., Wijbrans, J.R., 1998. Migration rate of volcanism along the Foundation Chain, SE Pacific. *Earth Planet. Sci. Lett.* 164, 41–59.
- Pan, Y., Batiza, R., 1998. Major element chemistry of volcanic glasses from the Easter seamount chain: constraints on melting conditions in the plume channel. *J. Geophys. Res.* 103, 5287–5304.
- Pariso, J.E., Sempéré, J.C., Rommevaux, C., 1995. Temporal and spatial variations in crustal accretion along the Mid-Atlantic ridge (29°–31°30'N) over the last 10 My: implications from a three-dimensional gravity study. *J. Geophys. Res.* 100, 17 781–17 794.
- Parker, R.L., 1972. The rapid calculation of potential anomalies. *Geophys. J. R. Astronom. Soc.* 31, 447–455.
- Phipps Morgan, J., Forsyth, D.W., 1988. 3-D flow and temperature perturbations due to a transform offset: effects on oceanic crust and upper mantle structure. *J. Geophys. Res.* 93, 2955–2966.
- Prince, R.A., Forsyth, D.W., 1988. Horizontal extent of anomalously thin crust near the Vema Fracture zone from three-dimensional analysis of gravity anomalies. *J. Geophys. Res.* 93, 8051–8063.
- Ribe, N., 1996. The dynamics of plume–ridge interaction: 2. Off-axis plumes. *J. Geophys. Res.* 101, 16 195–16 204.
- Ribe, N.M., Delattre, W.L., 1998. The dynamics of plume–ridge interaction—III. The effects of ridge migration. *Geophys. J. Int.* 133, 511–518.
- Sandwell, D.T., Smith, W.H.F., 1997. Marine gravity anomaly from Geosat and ERS1 satellite altimetry. *J. Geophys. Res.* 102, 10 039–10 054.
- Scheirer, D.S., Forsyth, D.W., Cormier, M.-H., Macdonald, K.C., 1998. Shipboard geophysical indications of asymmetry and melt production beneath the East Pacific Rise near the MELT experiment. *Science* 280, 1221–1224.
- Schilling, J.-G., 1973. Iceland Mantle plume: geochemical study of Reykjanes ridge. *Nature* 314, 62–67.
- Schilling, J.-G., 1985. Upper mantle heterogeneities and dynamics. *Nature* 314, 62–67.
- Schilling, J.G., 1991. Fluxes and excess temperatures of mantle plumes inferred from their interaction with migrating mid-ocean ridges. *Nature* 352, 397–403.
- Schilling, J.-G., Thompson, G., Kingsley, R., Humphris, S., 1985. Hotspot–migrating ridge interaction in the South Atlantic. *Nature* 313, 187–191.
- Small, C., 1995. Observations of ridge–hotspot interactions in the Southern Ocean. *J. Geophys. Res.* 100, 17 931–17 946.
- Sparks, D.W., Parmentier, E.M., Phipps Morgan, J., 1993. Three dimensional mantle convection beneath a segmented spreading center: implications for along axis variations in crustal thickness and gravity. *J. Geophys. Res.* 98, 21 977–21 972.
- Vogt, P.R., 1971. Asthenospheric motion recorded by the ocean floor south of Iceland. *Earth Planet. Sci. Lett.* 13, 153–160.
- Vogt, P.R., 1976. Plumes, subaxial pipe flow and topography along the mid-oceanic ridge. *Earth Planet. Sci. Lett.* 29, 309–325.
- Wang, X., Cochran, J.R., Barth, G., 1996. Gravity anomalies, crustal thickness and the pattern of mantle flow at the fast spreading East Pacific Rise, 9°–10°N: evidence for three-dimensional upwelling. *J. Geophys. Res.* 101, 17 927–17 950.
- Wessel, P., Smith, W.H.F., 1998. New improved version of Generic Mapping Tools released. *EOS Trans. AGU* 79 (47), 579.
- Wolfe, C.J., Bjarnson, I.T., VanDecar, J.C., Solomon, S.C., 1997. Seismic structure of the Iceland mantle plume. *Nature* 385, 245–247.